Geophysical Journal International

Geophys. J. Int. (2012) **190,** 278–292 doi: 10.1111/j.1365-246X.2012.05454.x

Lithosphere thickness and mantle viscosity inverted from GPS-derived deformation rates in Fennoscandia

S. Zhao,[1] K. Lambeck[2] and M. Lidberg[3]

[1] *Geoscience Australia, GPO Box* 378*, Canberra, ACT* 2601*, Australia. E-mail: jasonza99x@gmail.com*
[2] *Research School of Earth Sciences, The Australian National University, Canberra, ACT* 0200*, Australia*
[3] *Geodesy Department, Lantmaterigatan* 2*, SE*-801 82 *Gavle, Sweden*

Accepted 2012 March 8. Received 2012 March 8; in original form 2011 August 27

SUMMARY

Crustal deformation in Fennoscandia is associated with the glacial isostatic adjustment (GIA) process that is caused by ongoing stress release of the mantle after removal of the Late Pleistocene ice sheet by ∼10 cal ka BP. With an earth model of defined structure and rheology and an ice-sheet model of known melting history, the GIA process can be simulated by geophysical models, and the surface deformation rates can be calculated and used to compare with global positioning system (GPS) observations. Therefore, the crustal deformation rates observed by GPS in Fennoscandia provide constraints on the geophysical models. On the basis of two ice sheet models (ANU-ICE and ICE-5G) reconstructed independently by the Australian National University (ANU) and University of Toronto, we use the GPS-derived deformation rates to invert for lithosphere thickness and mantle viscosity in Fennoscandia. The results show that only a three-layer earth model can be resolved from current GPS data, providing robust estimates of effective lithosphere thickness, upper and lower mantle viscosity. The earth models estimated from inversion of GPS data with two different ice sheet models define a narrow range of parameter space: the lithosphere thickness between 93 and 110 km, upper mantle viscosity between 3.4 and 5.0 $\times$ 10^{20} Pa s, and lower mantle viscosity between 7 $\times$ 10^{21} and 13 $\times$ 10^{21} Pa s. The estimates are consistent with those inverted from relative sea-level indicators.

Key words: Space geodetic surveys; Transient deformation; Tectonics and climactic interactions; Rheology: mantle.

1 INTRODUCTION

A network of permanent global positioning system (GPS) stations was established in Fennoscandia to monitor regional deformation associated with glacial isostatic adjustment (GIA) under the auspices of the BIFROST project (The Baseline Inferences for Fennoscandian Rebound Observations Sea Level and Tectonics). Johansson *et al.* (2002) processed the GPS observations between 1993 and 2000 and investigated the pattern of 3-D crustal deformation in the region. Due to early development of the network, the observations before 1996 were affected by frequent disturbance in antenna environments and have 'jumps' in time series. Lidberg *et al.* (2007) provided an updated analysis of the GPS data of January 1996–June 2004 (Fig. 1). The uncertainties and systematic errors were reduced in the new solutions comparing with previous results (Johansson *et al.* 2002). A latest update of the deformation field is given by Lidberg *et al.* (2010) (Fig. 1).

The GPS-derived crustal deformation in Fennoscandia has been used to constrain GIA models (e.g. Milne *et al.* 2001). Both forward and inverse analyses of the surface deformation were conducted by Milne *et al.* (2004) and various earth models (lithosphere thickness estimates and depth-dependent mantle viscosity profiles) were investigated on the basis of the early GPS solutions of Johansson *et al.* (2002). Since the GPS network has been extended and data have been reprocessed (Lidberg *et al.* 2007, 2010), an updated modelling analysis with the new GPS solutions is necessary.

In addition, the ice sheet models used in previous modelling analyses (e.g. Milne *et al.* 2004) have been upgraded. The ice model developed at the Australian National University (named as ANU-ICE hereafter), which was used in previous studies (e.g. Lambeck *et al.* 1998; Milne *et al.* 2001, 2004), has been updated in a recent study (Lambeck *et al.* 2010). The ICE-5G model developed by Peltier's group at the University of Toronto has been released to replace ICE-3G (Peltier 2004).

In this study, we use the surface deformation rates derived by Lidberg *et al.* (2010) to invert for earth models associated with the GIA process in Fennoscandia, based on ANU-ICE and ICE-5G, respectively, and discuss the effects of uncertainties in ice sheets on inversion results.

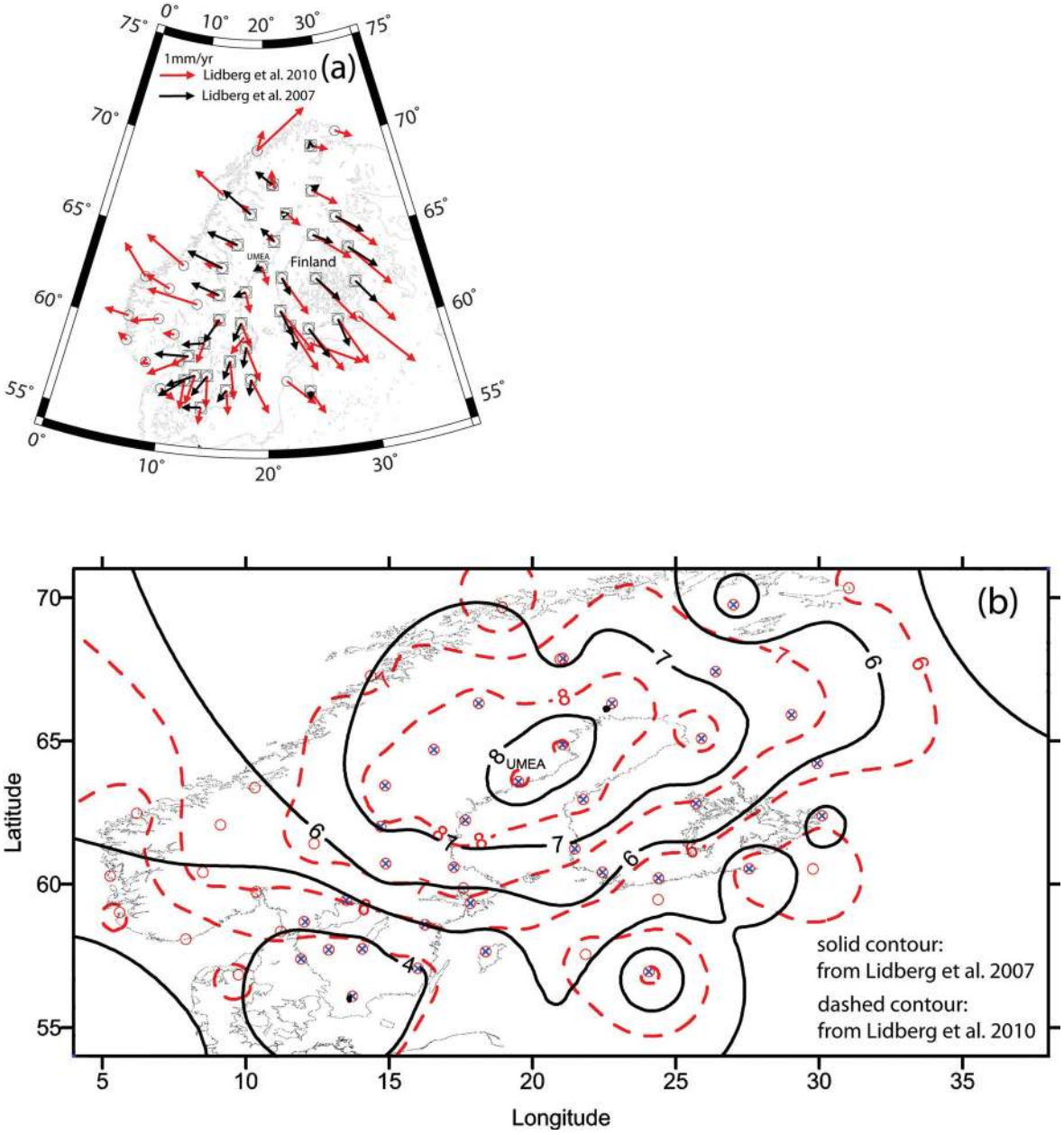

Figure 1. (a) Horizontal and (b) vertical deformation in Fennoscandia (unit: mm yr^{-1}). Black/solid arrows = observations from Lidberg *et al.* (2007), Grey/red arrows = observations from Lidberg *et al.* (2010) and error ellipses are ignored for clarity; solid and dashed contours in (b) denote vertical deformation from the 2007 (multiplication signs) and 2010 (circles) data, respectively.

2 GPS DATA

The GPS stations of the BIFROST project have an inter-station distance of 100–200 km (Fig. 1a). The data of January 1996–June 2004 were processed by Lidberg *et al.* (2007). This covered 8.5 yr compared to 6.5 yr for the previous published BIFROST solutions (Johansson *et al.* 2002). The time span for the individual station record is from 4.2 to 8.5 yr. The 'GAMIT/GLOBK' software package version 10.1 was used (Ref. Lidberg *et al.* 2007). The International Terrestrial Reference Frame (ITRF) realization was performed by constraining a number of globally distributed high-quality ITRF2000 stations (using their *a priori* ITRF2000 position and velocity values as well as their respective variance estimates). Therefore, the final solutions are dependent of the ITRF2000 velocity field globally. In other words, any distortion in ITRF2000 could be transferred to the regional solutions. For example, a shift in geocentre in ITRF2000 will affect the derived vertical velocity significantly, while horizontal velocities are less affected. A comprehensive description of the BIFROST project, including data analysis and results, is presented in Johansson *et al.* (2002) and Lidberg *et al.* (2007). Horizontal and vertical displacements at a total of 34 stations (squares in Fig. 1a) from Lidberg *et al.* (2007) are plotted in Fig. 1a (black/solid arrows) and Fig. 1b (solid/black contours), respectively. Stations in southern part of the region (e.g. Southern Denmark, Germany, Poland, etc.) are not used in this study because the magnitude of deformation on the stations is relatively small.

Table 1. Uncertainties in GPS-derived deformation.

Error	EW (mm)	NS (mm)	Vertical (mm)	Period (yr)
Nominal STD (averaged) (Lidberg *et al.* 2007)	±0.09	±0.07	±0.21	January 1996–June 2004
Nominal STD (averaged) (Lidberg *et al.* 2010)	±0.15	±0.10	±0.34	August 1993–November 2006
S_{du}*	±0.47	±0.45	±1.04	NA

*Estimated from the differences of two solutions (see Fig. 1).

The average nominal standard deviation (STD) is ±0.09 and ±0.07 mm for EW and NS displacement components, respectively, and ±0.21 mm for vertical displacement components (Table 1).

Lidberg *et al.* (2010) processed the data of August 1993–November 2006 for the extended BIFROST network (circles in Fig. 1). Horizontal and vertical displacements at a total of 54 stations are plotted in Fig. 1a (grey/red arrows) and Fig. 1b (dashed/red contours), respectively. Comparing with their 2007 solution, the 2010 solution has the following features: (1) the 2010 solution is constrained to ITRF2005; (2) there are more stations along the western coast of Norway, which improves the station coverage in the region; (3) the average nominal STD is increased to ±0.15 and ±0.10 mm for EW and NS displacement components, respectively, and ±0.34 mm for vertical displacement component (Table 1). Due to different observational periods, different (reference) coordinate systems and different data processing procedures used, there are significant differences in the derived deformation fields (Fig. 1). The horizontal displacements from the 2010 solution (red/grey arrows) are generally larger than those from the 2007 solution (black/solid arrows), except for several stations in central Sweden (west of UMEA). Also, the vertical displacements from the 2010 solution (dashed contours) are larger than those of the 2007 solution (solid contours). For example, the extent of the area with uplift more than 8 mm is larger than that of the 2007 solution.

For the 2010 solution, the regional BIFROST analysis is combined with a global network analysis, and the daily combined networks were stabilized to the ITRF2005 (Ref. Lidberg *et al.* 2010 for details). This is different from the strategy used for the 2007 solution, where the solution was combined with networks from the Scripps Orbit and Permanent Array Center (SOPAC), and constrained to ITRF2000 (Lidberg *et al.* 2007).

ITRF2000 and ITRF2005 are defined by the centre of mass of Earth's system (CM) (Altamimi *et al.* 2002, 2003; 2011). The GIA models are referenced to the centre of mass of solid Earth (CE). Argus (2007) has revealed a difference of 1.8 mm yr^{-1} in the z-direction between ITRF2000 and ITRF2005 relative to CE. The estimate of CE (with a formal error ∼0.8 mm yr^{-1}) is inferred with data from satellite laser ranging (SLR), very long baseline interferometry (VLBI), Doppler orbitography and radiopositioning integrated by satellite (DORIS) and GPS together with a global GIA model (Argus 2007). The difference between ITRF2000 and ITRF2005 is mostly reflected in vertical components (Altamimi *et al.* 2007). In addition, Wu *et al.* (2010) found that the origin (CM) of ITRF2005 is in agreement with CE at the level of ∼1 mm yr^{-1}, which is consistent with results from Argus & Peltier (2010).

In general, the differences between the 2007 and 2010 solutions reflect combined errors in the GPS observations, which are related to observational noise, reference systems, and data processing procedures. Although it is difficult to quantify the error sources accurately, the differences between two solutions can be used as a good measure to the current accuracy of derived displacements. Let the differential vector of two solutions be $\mathbf{du}$ ($= \mathbf{u}_1 - \mathbf{u}_2$), the STD $S_{\mathbf{du}}$ of $\mathbf{du}$ is given by

$$(S_{du})^2 = \left(\sum_1^n (\mathbf{du}_i)^2\right) \Big/ n - 1, \tag{1}$$

where n is the total number of the common stations between two solutions ($n = 34$ used here). Since any systematic errors common in both solutions are eliminated in the differential vector ($\mathbf{du} = \mathbf{u}_1 - \mathbf{u}_2$), there is a possibility that S_{du} underestimates systematic errors in the GPS data, though this is difficult to verify.

The STDs estimated from the differences of two solutions and their nominal error estimates are listed in Table 1. The estimated STD of the vertical component is ±1.04 mm, which is about twice that of horizontal components (±0.47 and ±0.45 mm). This indicates that current accuracy in vertical components is about a factor of 2 less than those of horizontal components. Comparing the nominal STDs of the 2010 solution (±0.15, ±0.10, and ±0.34 mm) with those derived from the differences of two solutions (±0.47, ±0.45, and ±1.04 mm), the nominal STDs have underestimated the real errors by a factor of about 3.

The vertical displacements (using 2010 solution hereafter) display a dome shape of uplift with a maximum value of 11.1 mm yr^{-1} at site UMEA. The horizontal displacements show a radial pattern with points moving away from the uplift centre. The maximum horizontal component is 1.5 mm yr^{-1}, which is about seven times smaller than the maximum vertical component. These results confirm that crustal extension is one of the mechanisms associated with post-glacial rebound in the region, which is consistent with previous studies (e.g. Milne *et al.* 2004).

3 POST-GLACIAL REBOUND MODEL

3.1 Basic formulae

The solution of the post-glacial deformation equation uses the correspondence principle to transfer elastic solutions to viscoelastic solutions and then obtaining the inverse of the Laplace transform (Peltier 1974; Peltier & Andrews 1976; Wu & Peltier 1982; Peltier 1985; Nakada & Lambeck 1987). The model used in this study calculates the responses of a spherically symmetric (Maxwell) viscoelastic earth model to a load composed of a model of Late Pleistocene ice cover and a gravitationally self-consistent ocean load (Lambeck & Johnston 1998). The displacement vector $\mathbf{u}(r, \theta, \lambda)$ in a spherical coordinate system for $r < R$ is given by

$$\mathbf{u}(r, \theta, \lambda) = \sum_n \frac{\psi_{1,n}(r)}{g^{(0)}(r)} \left(\frac{r}{R}\right)^n \left[h_n(r) Y_n(\theta, \lambda) \hat{r} + r l_n(r) \nabla Y_n(\theta, \lambda)\right], \tag{2}$$

where ∇Y_n is the gradient of the spherical-harmonic function; h and l are the displacement Love numbers, and k is the potential Love number; $\psi_{1,n}(r)$ is the gravitational potential; $g^{(0)}(r)$ is the initial gravity; R is the earth radius; $\hat{r}$ is the unit radial vector; θ is the colatitude and λ is the longitude.

In the computation, the effects of Earth's rotation and water/ocean load are also included (Sabadini & Vermeersen 1997; Mitrovica & Milne 1998; Johnston & Lambeck 1999). More details of the computation aspects are discussed in Johnston & Lambeck (1999), Lambeck *et al.* (2003), and Milne *et al.* (2004). This package of programs and models has been successfully used to interpret sea-level indicators, reconstruct ice sheets and test earth models in many separate studies (e.g. Lambeck *et al.* 1998; Lambeck & Johnston 1998; Fleming & Lambeck 2004). Although there is trade-off between ice sheets and earth models in the GIA modelling analysis, previous studies with limited observational data have provided consistent solutions (Ref. Peltier 2004; Lambeck *et al.* 2010). A recent trend is to consider Earth's heterogeneity and non-linear mantle rheology in post-glacial rebound modelling (Steffen & Wu 2011). In this study, we limit models to the linear rheology and ignore the effects of lateral change in earth structures.

3.2 Earth models

Since modern surface deformation rates are not sensitive to detailed ice melting histories, the GPS data do not have resolving power for earth models of more than three layers (discussed later). Due to this limitation, only results associated with earth models of three and four layers are reported in details. The three-layer model, as shown in Fig. 2a, consists of a lithosphere layer, an upper mantle (<670 km) and a lower mantle between 670 and 2891 km. In the four-layer model (Fig. 2b), a transition zone is introduced between 400 and 670 km, and the upper mantle is set between the base of the lithosphere and the depth of 400 km. Values for the density and bulk and shear moduli as a function of depth are from the preliminary reference earth model (PREM) of Dziewonski & Anderson (1981). A basic assumption used in this study is that lateral variability in mantle parameters on the scale of the area considered can be ignored. The lithosphere thickness and the viscosity of each layer are free parameters in inversion analysis.

There are many occasions where uncertainties in sea-level indicators are large so that a three-layer model is used as a guide, and more sophisticated earth models (viscosity profiles) cannot be resolved (e.g. Vink *et al.* 2007; Lambeck *et al.* 2010). Therefore, the three-layer earth model is most commonly used in relative sea-level analysis (e.g. Lambeck & Purcell 2005), and it is practically significant to accurately determine its model parameters. The four-layer model in this study is used to test whether it provides a better fit to the GPS observations by including a transition zone.

3.3 Ice sheet models

Two ice sheet models are used in this study: ANU-ICE and ICE-5G. Both ice sheet models were mainly constrained by relative sea-level indicators and glacial morphological data. A recent update for the ANU-ICE model is given by Lambeck *et al.* (2010), and details about construction of the ICE-5G model and its predecessors have been discussed in several studies (e.g. Tushingham & Peltier 1991; Peltier 2002; Peltier 2004). To explore the differences between these two ice sheet models, contours of ice thickness at $t = 20$ cal ka BP in Fennoscandia are given in Fig. 3.

Two profiles are shown in Fig. 4 for ice distribution along the 62° parallel and 20° meridian, respectively (also see Fig. 3). Comparing Figs 4a and b, it is clear that both ice sheet models give a dome shape of ice coverage. The ice contour of 2000 m in ICE-5G extends further east than ANU-ICE (Fig. 3), while the ice contours of 1000 and 1500 m in ANU-ICE extend further south. That is, there is more ice in ICE-5G in the eastern part of the region (Fig. 4a), while in the south, there is more ice in ANU-ICE (Fig. 4b).

Fig. 5 shows the history of ice melting at the location (20°, 62°) since the last glacial maximum (LGM) from the two ice sheet models. Ice melting occurred faster in ANU-ICE than in ICE-5G. For example, at $t = 15$ cal ka BP, the ice thickness in ANU-ICE dropped from about 3000 to 1000 m, while the ice thickness in ICE-5G is still above 2000 m. The total volume of ice melted since 40 cal ka BP in ICE-5G is about twice of that in ANU-ICE. Note that modern surface deformation associated with post-glacial rebound in Fennoscandia is mainly influenced by the ice volume and distribution after LGM (between 10 and 20 cal ka BP). Therefore, the difference between two ice sheets is mainly reflected by the melting curve between 10 and 20 cal ka BP (Fig. 5), which indicates that there is about 20 per cent more ice in ICE-5G than in ANU-ICE.

The ice sheet models are usually used in conjunction with a set of earth models in GIA-related sea-level and deformation studies. Such as the ICE5G is coupled with the earth model VM2, which is equivalent to a model with a lithosphere thickness of 90 km, an upper mantle viscosity of 5×10^{20} Pa s and an averaged lower mantle viscosity of 1.6×10^{21} Pa s (Peltier 2004; Braun *et al.* 2008; Argus & Peltier 2010). Obviously, using different ice sheet models

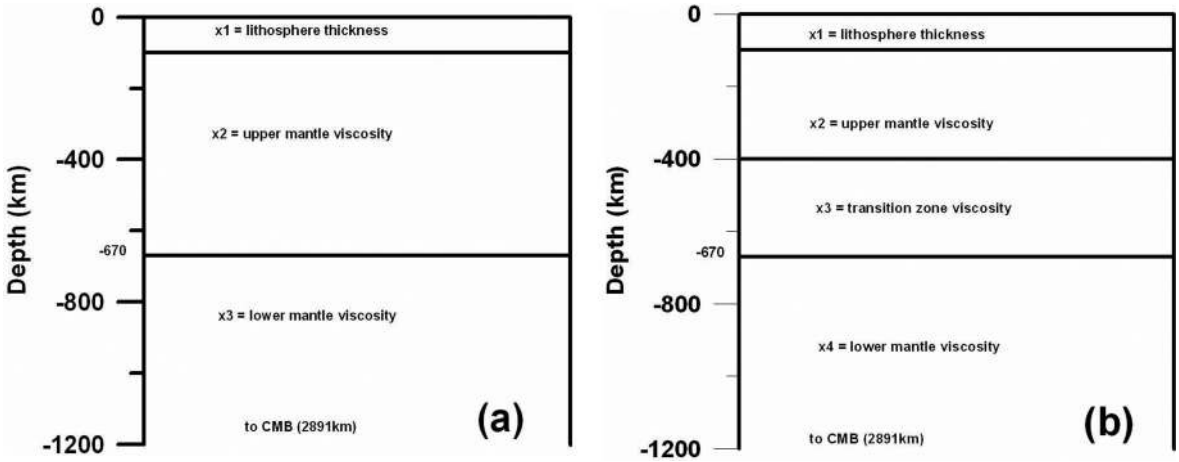

Figure 2. Two representative earth models used in the study. (a) Three-layer model. (b) Four-layer model (with a transition zone). x_i are the unknown parameters in the inversion computation ($i = 1, 2, 3, 4$).

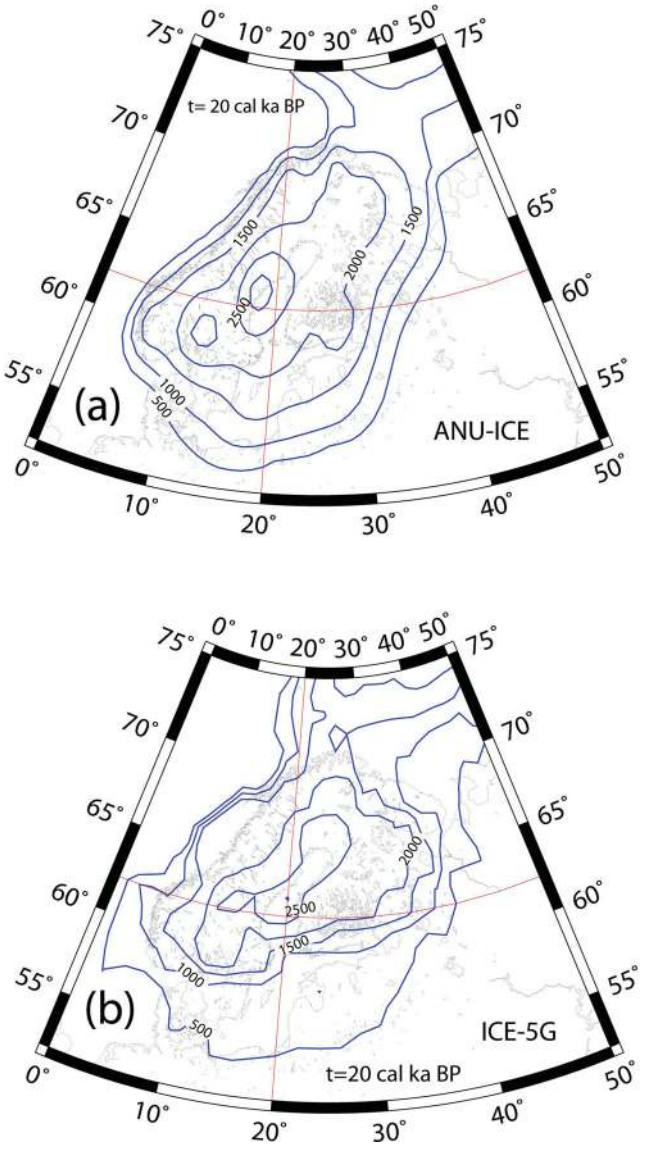

Figure 3. Contours of ice thickness (unit: m) in Fennoscandia at $t = 20$ cal ka BP for (a) ANU-ICE and (b) ICE-5G, respectively. The 62° parallel and 20° meridian indicate the positions of two profiles in Fig. 4.

in the inversion analysis will affect the earth model parameters estimated from GPS data. To explore the effects, the inversion analysis of GPS data is conducted with these two ice sheet models, respectively. Since the ice sheet models are not constrained by surface deformation data, the inversion analysis of GPS data could provide an independent examination of the ice sheets or/and earth models to a certain degree.

4 INVERSION METHOD

Schematically, deformation u_i ($i = 1$, 2 and 3) at a point (λ, θ) on the Earth's surface associated with post-glacial rebound can be expressed as

$$u_i(\lambda, \theta) = \mathbf{f}(\mathbf{Me}, \mathbf{Mc}), \tag{3}$$

where **Me** is the earth model, **Mc** is the ice sheet model, and **f** is the nonlinear operator. Detailed expressions are given by formulae (2) (Lambeck & Johnston 1998).

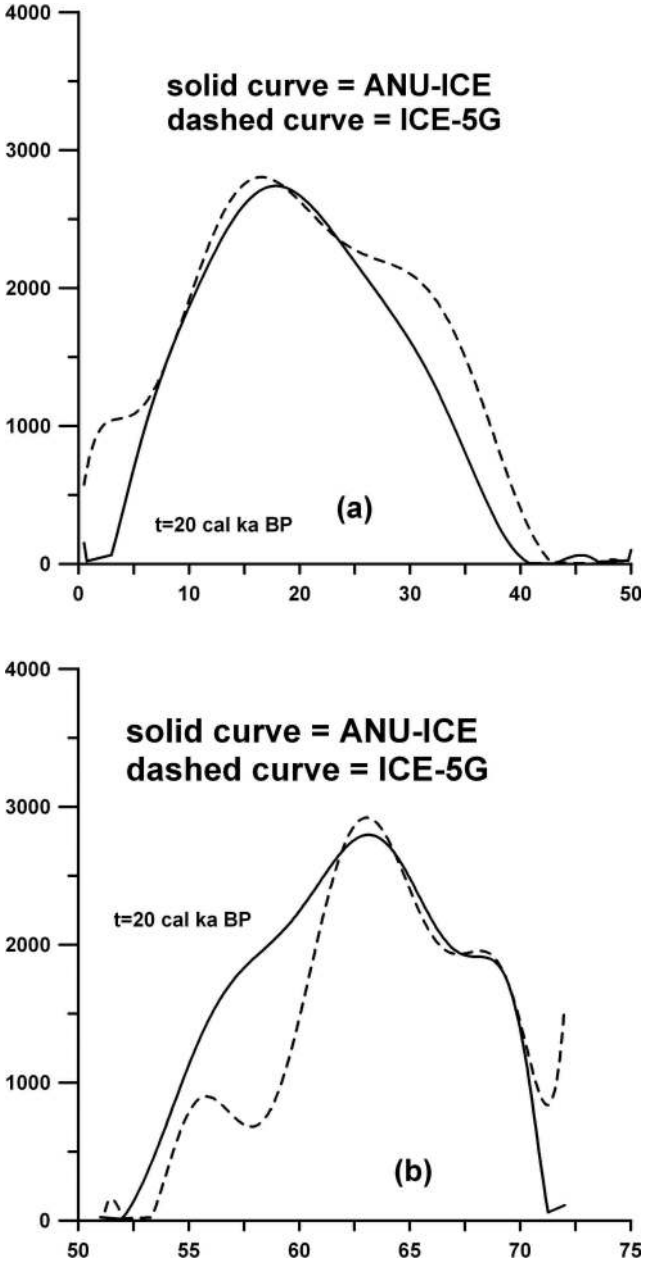

Figure 4. Ice thickness at $t = 20$ cal ka BP along two profiles (see Fig. 3) for ANU-ICE (solid curve) and ICE-5G (dashed curve), respectively. (a) West–east profile at latitude = 62° and (b) south–north profile at longitude = 20°.

Given ice sheet models, the earth model parameters (**Me**) can be estimated by the inversion of the displacements. The displacements vector of GPS points resulting from post-glacial rebound can be expressed as

$$\mathbf{u} = \mathbf{F}(\mathbf{Me}), \tag{4}$$

where **F** is the nonlinear operator that relates **u** to **Me**.

With the inverse operator $\mathbf{F}^{-1}$, the earth model can be expressed as

$$\mathbf{Me} = \mathbf{F}^{-1}(\mathbf{u}). \tag{5}$$

The corresponding mathematical model for solving the nonlinear inverse problem is given by

$$\left\| \{\mathbf{u_0} - \mathbf{F}(\mathbf{Me})\} / \boldsymbol{\sigma} \right\| = \min \left\| \right. \tag{6}$$

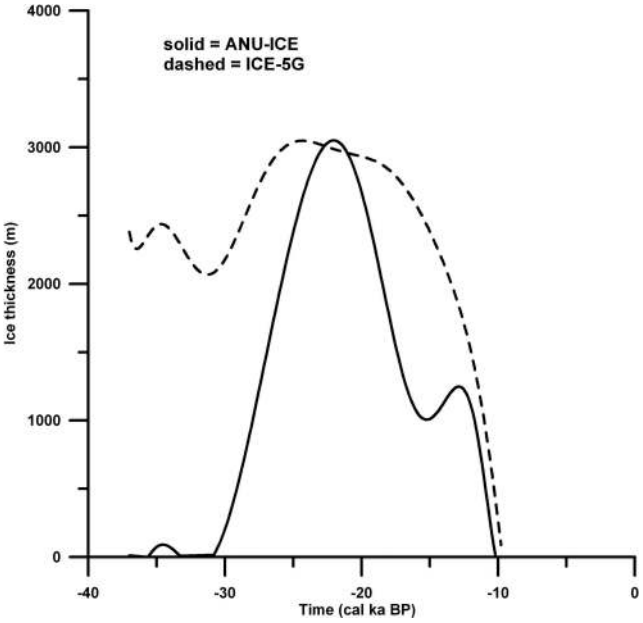

Figure 5. Ice melting history during LGM in Fennoscandia at longitude = 20° and latitude = 62° from ANU-ICE (solid curve) and ICE-5G (dashed curve), respectively.

subject to $C_1 \leq \mathbf{Me} \leq C_2$, where $\|.\|$ denotes the L_2 norm, $\mathbf{u}_0$ and $\boldsymbol{\sigma}$ are the observed deformation (rate) vector and its STD, respectively, **Me** is the unknown earth model parameter vector and C_1 and C_2 are the lower and upper limits of the parameter vector, respectively. The solution of the model (6) can be obtained by a nonlinear programming method (Gabasov & Kirillova 1988).

To test the effect of the inversion method on estimating model parameters from surface deformation rates, several numerical tests have been done (not shown here). The tests indicate that the inversion algorithm is robust and not affected by any systematic and gross errors in signals/observations. The parameter space of the earth models is set to be:

50 km $\leq$ lithosphere thickness $\leq$ 150 km

0.1×10^{20} Pa s $\leq$ upper mantle viscosity $\leq 100 \times 10^{20}$ Pa s,

0.1×10^{20} Pa s $\leq$ transition zone viscosity $\leq 100 \times 10^{20}$ Pa s,

0.1×10^{20} Pa s $\leq$ lower mantle viscosity $\leq 800 \times 10^{20}$ Pa s.

The misfit to the GPS data is calculated with

$$\sigma_p^2 = \frac{1}{n_0 - t_0} \sum_{k=1}^{n_0} \left(\frac{u_k^{\mathrm{GPS}} - u_k^m}{\sigma_k} \right)^2, \tag{7}$$

where σ_p is the weighted STD of residuals, $u_k{}^{\mathrm{GPS}}$ and $u_k{}^{\mathrm{m}}$ are observed and modelled displacements, respectively, σ_k is the STD of the k_{th} observation ($k = 1, 2, 3, \ldots, n_0$), n_0 is the number of observations and t_0 is the number of earth model parameters. Theoretically, σ_p should approach 'unit' if the residuals are subject to a standard normal distribution, and there are no un-modelled signals and systematic errors in observations.

5 INVERSION RESULTS

The GPS data from Lidberg *et al.* (2010) have been used to invert for earth model parameters. Inversion computation is done for horizontal and vertical displacements separately and jointly, respectively. For each GPS data set (horizontal, vertical and both), the inversion analysis is conducted for different earth models (viscosity profiles) with different ice sheet models (ANU-ICE and ICE-5G). The purpose of using different data sets with different ice sheet models in the inversion analysis is to examine the contribution of each data type, and effects of uncertainties in ice sheets on the estimated earth model parameters. The parameters estimated for the three- and four-layer earth models are given in Tables 2 and 3, respectively.

5.1 Results for the three-layer earth model

The lithosphere's effective elastic thickness of the three-layer earth model estimated from different data sets is within a small range: about 93–97 km for ANU-ICE and 105–110 km for ICE-5G (Table 2). The estimate of the upper mantle viscosity for different data sets is in the range of 4.9×10^{20}–5.0×10^{20} Pa s for ANU-ICE and 3.4×10^{20}–4.0×10^{20} Pa s for ICE-5G. There is a difference in the lower mantle viscosity estimated from different data with ANU-ICE: the estimate of 131.5×10^{20} Pa s from vertical displacements (Model A2) is about twice of that (70.0×10^{20} Pa s) from the horizontal data (Model A1). For ICE-5G, the lower mantle

Table 2. Inversion results for the three-layer earth model.

GPS data	Ice model	Lithosphere thickness (km)	Upper mantle viscosity (10^{20} Pa s)	Lower mantle viscosity (10^{20} Pa s)	RSTD	Notes
Horizontal	ANU-ICE	97 ± 8	4.9 ± 1.2	70.0 ± 15	±1.151	Model A1
Vertical	ANU-ICE	95 ± 2	5.0 ± 1.0	131.5 ± 31	±1.203	Model A2
Joint inversion	ANU-ICE	93 ± 12	5.0 ± 1.4	122.0 ± 27	±1.158	Model A3
Horizontal	ICE-5G	110 ± 8	4.0 ± 0.9	50.0 ± 15	±1.127	Model B1
Vertical	ICE-5G	105 ± 11	3.4 ± 0.4	78.8 ± 25	±1.393	Model B2
Joint inversion	ICE-5G	106 ± 12	3.5 ± 0.3	72.6 ± 24	±1.228	Model B3

Table 3. Inversion results for the four-layer earth model.

GPS data	Ice model	Lithosphere thickness (km)	Upper mantle viscosity (10^{20} Pa s)	Transition zone viscosity viscosity (10^{20} Pa s)	Lower mantle viscosity (10^{20} Pa s)	RSTD	Notes
Horizontal	ANU-ICE	105 ± 13	3.7 ± 1.2	18.0 ± 3.9	93.7 ± 45	±1.137	Model C1
Vertical	ANU-ICE	87 ± 20	4.0 ± 0.7	5.7 ± 3.4	160.9 ± 80	±1.223	Model C2
Joint inversion	ANU-ICE	100 ± 9	4.1 ± 1.5	6.0 ± 2.8	164.4 ± 77	±1.174	Model C3
Horizontal	ICE-5G	109 ± 11	3.8 ± 1.2	7.8 ± 3.7	64.9 ± 60	±1.126	Model D1
Vertical	ICE-5G	112 ± 33	3.5 ± 1.2	2.7 ± 2.3	139.9 ± 62	±1.385	Model D2
Joint inversion	ICE-5G	112 ± 26	3.5 ± 1.2	2.8 ± 2.4	139.9 ± 80	±1.231	Model D3

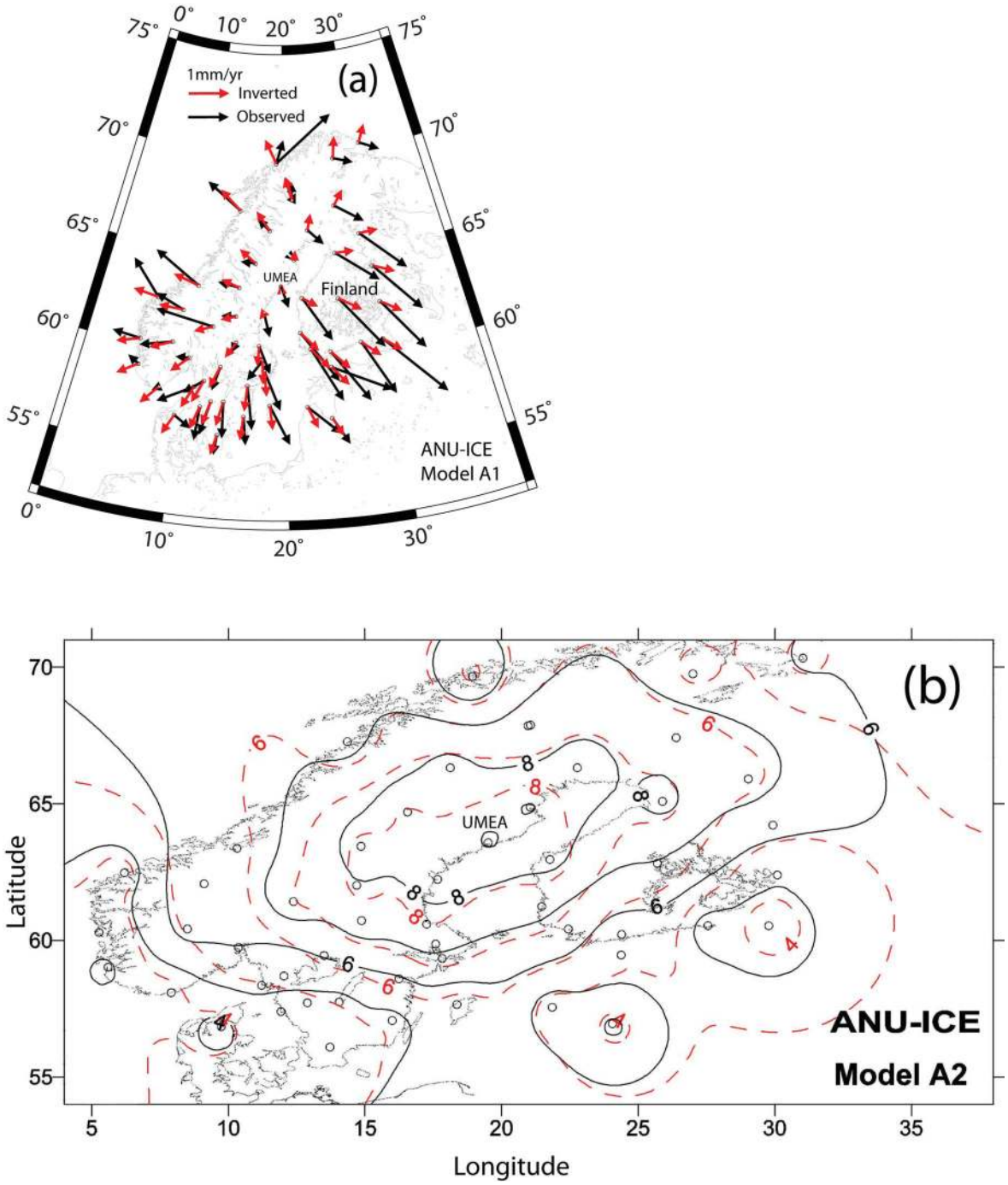

Figure 6. (a) Horizontal and (b) vertical displacements predicted by ANU-ICE with the three-layer earth model from inversion of horizontal (Model A1) and vertical deformation (Model A2), respectively (solid contours = observations; dashed contours = predictions; unit: mm yr^{-1}).

viscosity estimated from different data set is in the range of 50.0 × 10^{20}–78.8 × 10^{20} Pa s.

The results from the joint inversion are similar to those from inversion of vertical deformation, suggesting that the joint inversion computation is dominated by the vertical deformation. This is mainly due to the larger signal-to-noise ratio of the vertical deformation, comparing with that of horizontal deformation. The average vertical deformation is about 6.2 mm with the averaged STD of about ±1.0 mm (Table 1), which gives a signal-to-noise ratio of about 6.2:1. For the horizontal deformation, the average signal level is about 0.59 mm with the averaged STD of about ±0.45–0.47 mm, which gives a signal-to-noise ratio of approximately 1.3:1. This demonstrates that the weight of vertical deformation is about five times that of the horizontal deformation in the joint inversion. Several inversion experiments show that the effects of change in the weight ratio between horizontal and vertical displacements do not alter the estimated earth model parameters significantly.

The differences of the two ice models result in differences in the estimated earth models. For model parameters (Models B1 and B2)

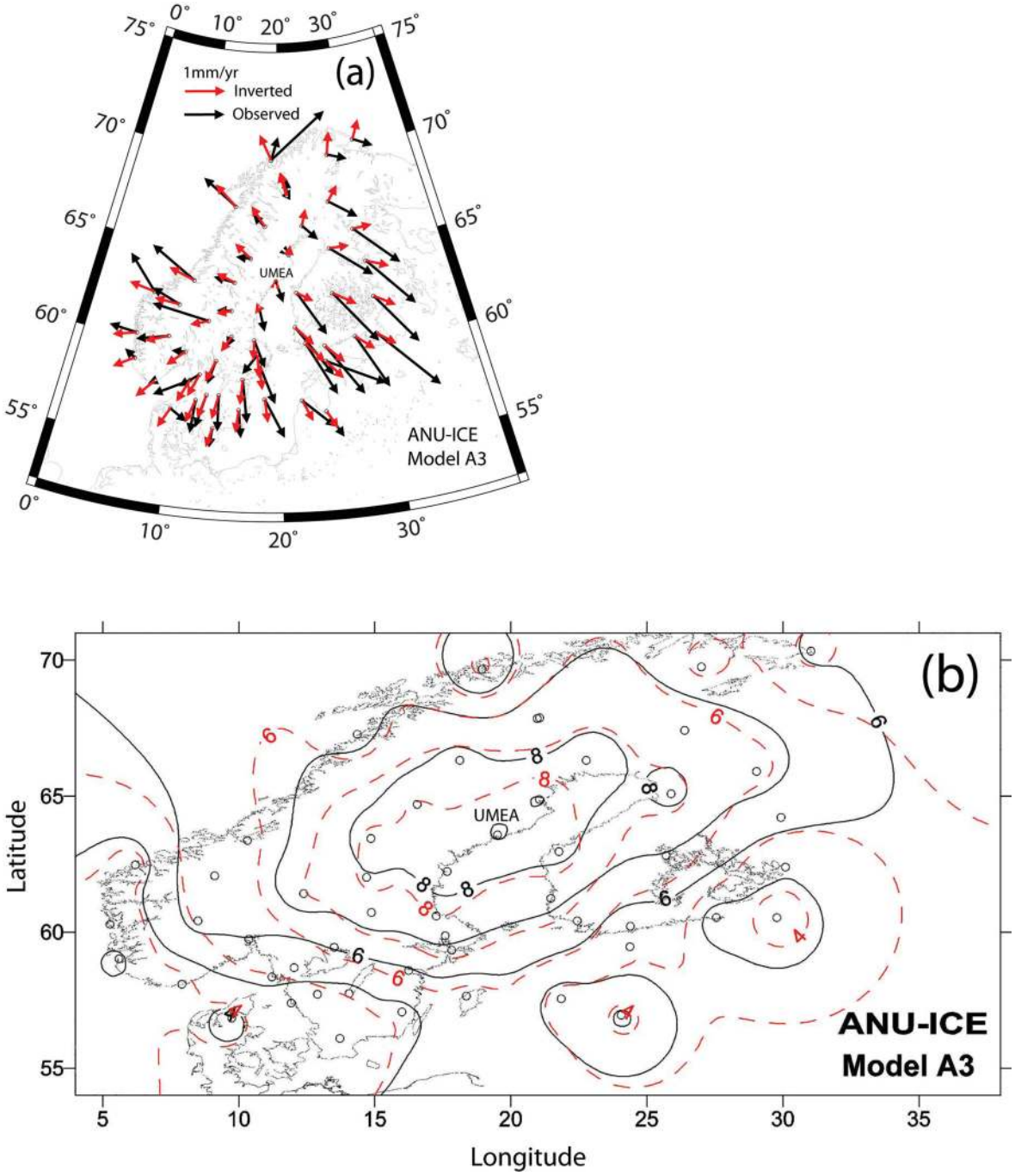

Figure 7. (a) Horizontal and (b) vertical displacements predicted by ANU-ICE with the three-layer earth model from joint inversion (Model A3) of horizontal and vertical deformation (solid contours = observations; dashed contours = predictions; unit: mm yr^{-1}).

estimated with ICE-5G, the lithosphere thickness (105–110 km) is about 10 km larger than that (95–97 km) of ANU-ICE (Models A1 and A2), and the lower mantle viscosity estimate (50×10^{20}–78.8×10^{20} Pa s) is significantly smaller than that (70.0×10^{20}–131.5×10^{20} Pa s) from ANU-ICE.

For ANU-ICE, the predicted horizontal and vertical displacements are plotted in Figs 6a and b, respectively (Models A1 and A2). There are some notable differences between the observed and predicted horizontal vectors, especially in the southeast part of the region (South Finland), where the predicted horizontal displacements are smaller than those observed. The observed and predicted vertical displacements are in general agreement with the predicted uplift centre near site UMEA, which is consistent with observations. The results from joint inversion with ANU-ICE give similar results (Fig. 7). Judging from the weighted residual STDs (RSTD) of Models A2 and B2 (± 1.203 versus ± 1.393), the ANU-ICE model provides a better fit to the vertical displacements.

For ICE-5G, the predicted horizontal and vertical displacements are plotted in Fig. 8. Model B2 from inversion of vertical displacements (Fig. 8b) with ICE-5G predicted the uplift centre in the east of site UMEA, which is not consistent with observations (solid contours). The results from joint inversion with ICE-5G give

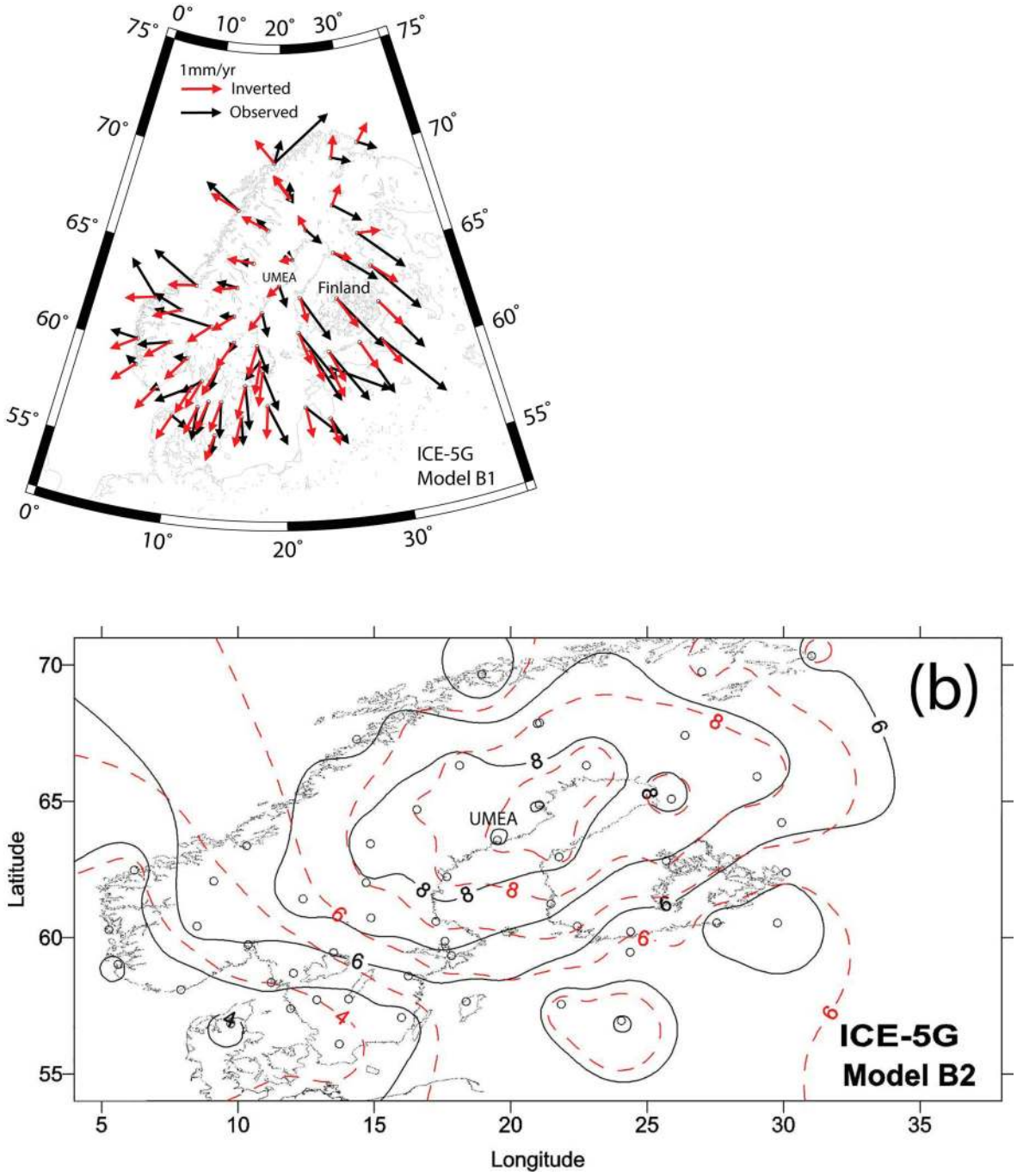

Figure 8. (a) Horizontal and (b) vertical displacements predicted by ICE-5G with the three-layer earth model from inversion of horizontal (Model B1) and vertical deformation (Model B2), respectively (solid contours = observations; dashed contours = predictions; unit: mm yr^{-1}).

a similar result (Fig. 9): the predicted area of 8 mm uplift (dashed contour) shifted to east, comparing with that (solid contour) concentrated at site UMEA from observations (Fig. 9b). The discrepancy from observations is due to the centre of the ice sheet (with the maximum ice height) located at the northeast of site UMEA in ICE-5G.

The ICE-5G predicted slightly larger horizontal deformation in the southeast part of the region (South Finland; Fig. 8a), which provides an improved fit to the horizontal displacements (Mode B1), comparing with those predicted by ANU-ICE (Model A1). The RSTD (±1.127) from the inversion computation with horizontal displacements is slightly less than that (±1.151) from the ANU-ICE. As shown in Fig. 4a, there is more ice in the eastern part of the region in ICE-5G than in ANU-ICE. In addition, there is more ice presented between 10 and 20 cal ka BP in ICE-5G (Fig. 5). These differences lead to a slightly large magnitude of horizontal deformation predicted with ICE-5G for the southeast part of the region. In general, uncertainties in ice models and errors in GPS observations both contribute to the varied estimates of the model parameters.

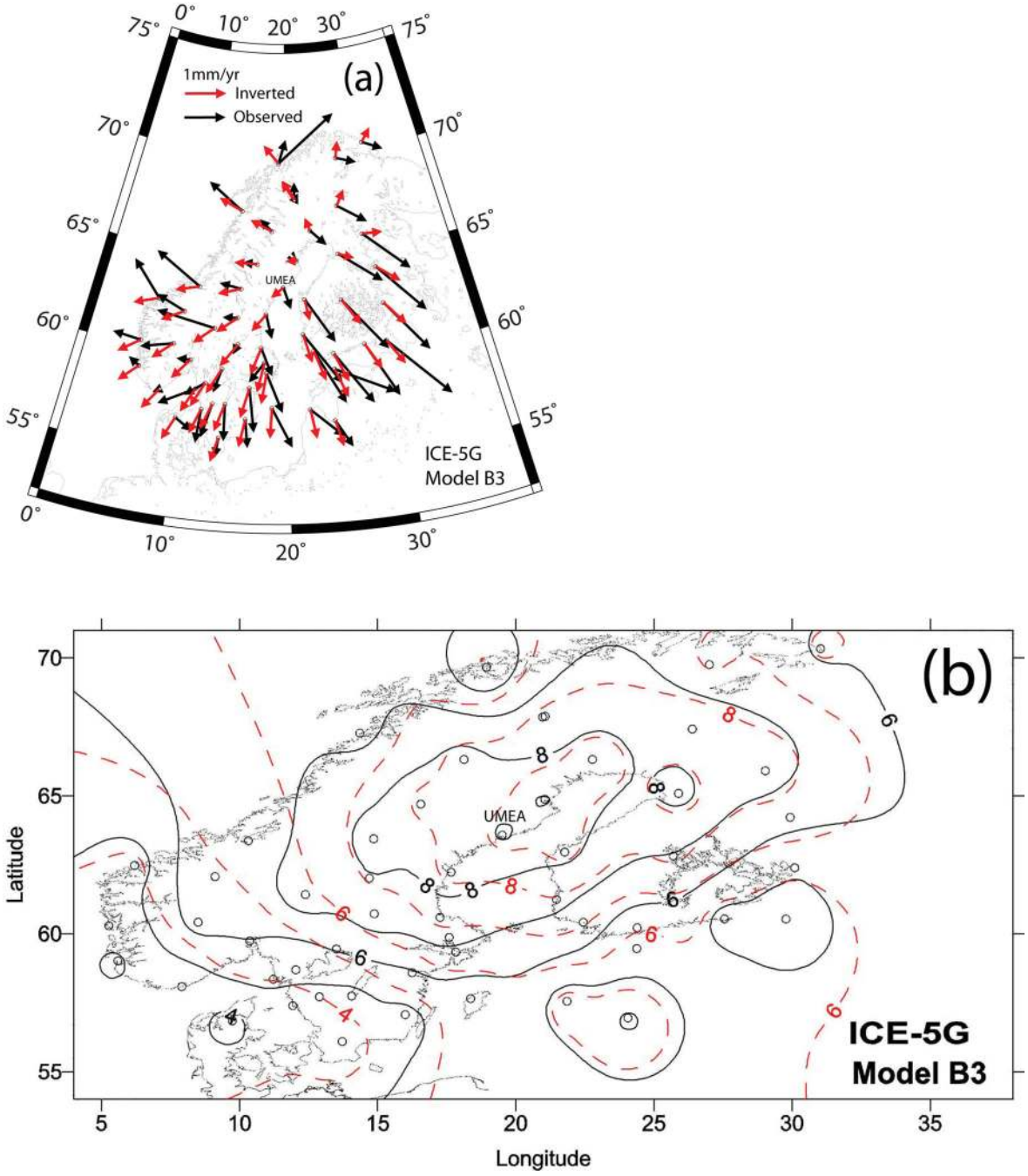

Figure 9. (a) Horizontal and (b) vertical displacements predicted by ICE-5G with the three-layer earth model from joint inversion (Model B3) of horizontal and vertical deformation (solid contours = observations; dashed contours = predictions; unit: mm yr^{-1}).

5.2 Results for the four-layer earth model

The predicted horizontal and vertical displacements with the four-layer earth model are plotted in Figs 10 and 11. Comparing results from Tables 2 and 3, the following features are observed:

(1) For horizontal deformation, adding a transition zone has no significant effect on estimates of earth model parameters (Models A1 versus C1; Models B1 versus D1), though there is a 6–8 km difference in lithosphere thickness estimates. There are no notable differences between the horizontal displacements predicted by the three- and four-layer earth models from inversion of horizontal deformation (Figs 6a versus 10a and Figs 8a versus 11a). The RSTD of horizontal displacements from the four-layer earth model is ±1.137 and ±1.126 for ANU-ICE and ICE-5G (Models C1 and D1), respectively, which are slightly reduced, comparing with those (±1.151; ±1.127) from the three-layer models (Models A1 and B1).

(2) For vertical deformation, the lower mantle viscosity estimates of the four-layer earth models are larger than those of three-layer models. For ANU-ICE, the estimate changed from 131.5×10^{20} to 160.9×10^{20} Pa s (Model A2 versus Model C2), and from 78.8×10^{20} to 139.9×10^{20} Pa s; (Model B2 versus Model D2) for ICE-5G. The Model D2 from ICE-5G produced a small area of uplift in the east of UMEA (dashed contour of 9 mm), which over-estimates

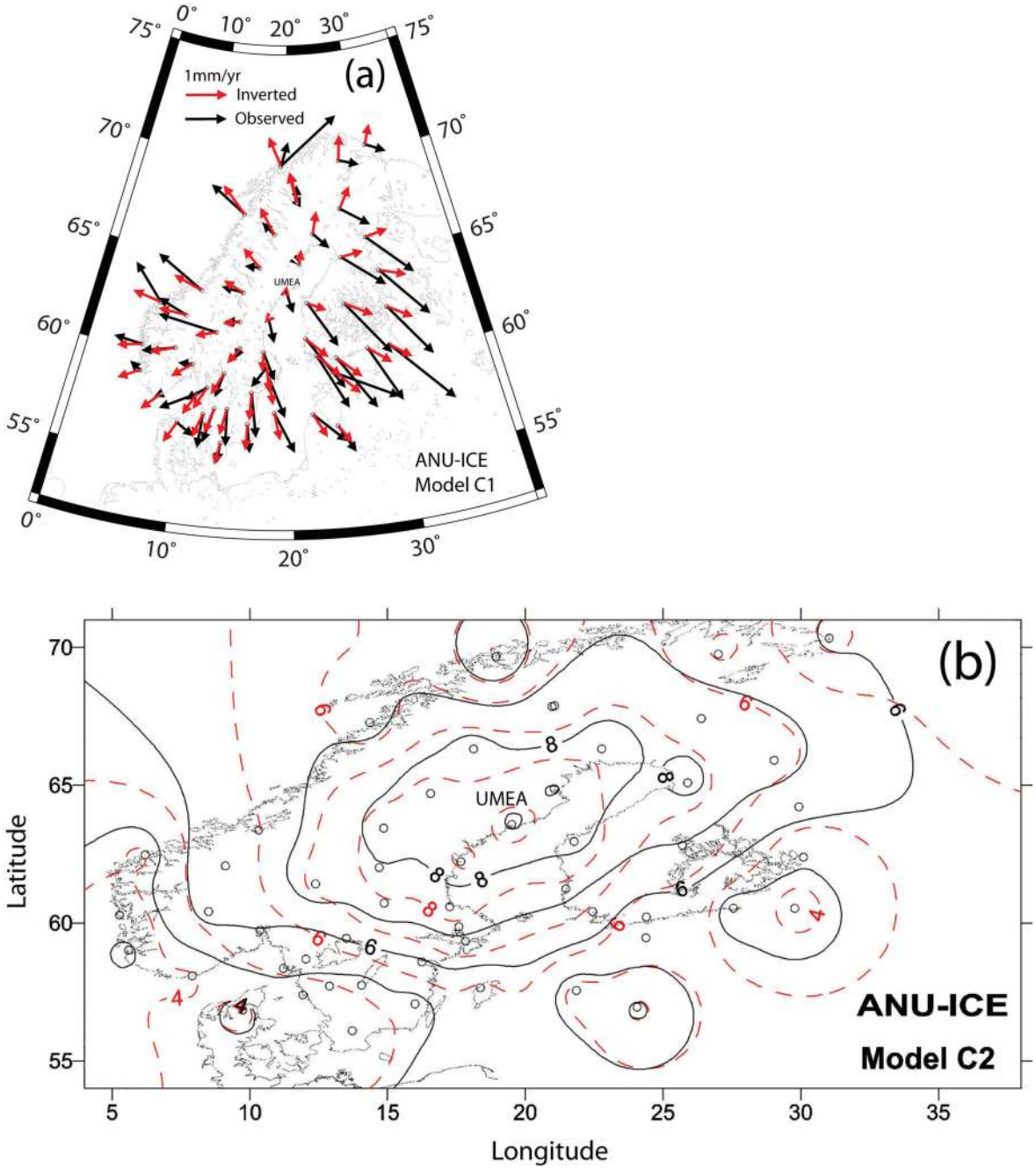

Figure 10. (a) Horizontal and (b) vertical displacements predicted by ANU-ICE and the four-layer earth model (models C1 and C2) from inversion of horizontal and vertical deformation, respectively (solid contours = observations; dashed contours = predictions; unit: mm yr^{-1}).

vertical displacements by about 1 mm (Fig. 11b). The residual STD of vertical displacements from the four-layer earth model is ±1.223 and ±1.385 for ANU-ICE and ICE-5G (Models C2 and D2), respectively. These error estimates are not significantly different to those (±1.203; ±1.393) from the three-layer models (Models A2 and B2).

(3) The model parameters estimated from the joint inversion are similar to those from vertical deformation, but the residual STDs are smaller than that from vertical deformation alone, due to constraints from the horizontal deformation. The lithosphere thickness estimated from different data sets is in the range of 87–105 km for ANU-ICE, and of 109–112 km for ICE-5G. It is worth noting that there is a 25 km difference in the lithosphere thickness estimated from inversion of vertical displacements between ANU-ICE and ICE-5G (Models C2 versus D2), and a ∼17 km difference between horizontal and vertical deformation with ANU-ICE (Models C1 and C2). Comparing the effects of using different ice sheet models with those of using different data sets, it is clear that the effects of different ice sheet models (e.g. Models C3 versus D3) are comparable to those from errors in GPS observations (e.g. Models C1 versus C2).

(4) The viscosity for the transition zone estimated from vertical displacements (Models C2 and D2) is in the range of 2.7–5.7 ($\times 10^{20}$ Pa s), which are similar to upper mantle viscosity estimates of 3.5–4.0 ($\times 10^{20}$ Pa s). The estimates of the transition zone viscosity

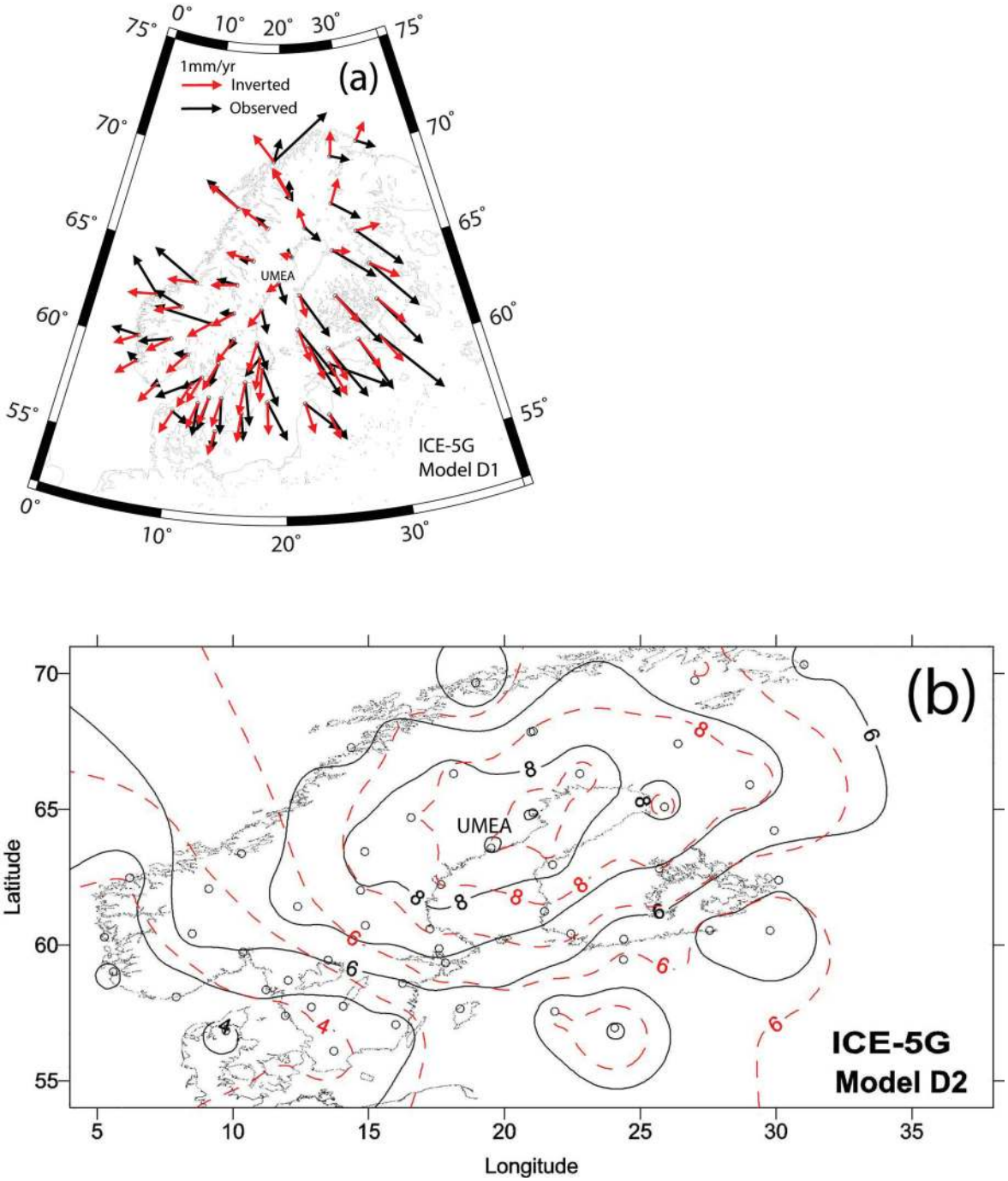

Figure 11. (a) Horizontal and (b) vertical displacements predicted by ICE-5G and the four-layer earth model (models D1 and D2) from inversion horizontal and vertical deformation, respectively (solid contours = observations; dashed contours = predictions; unit: mm yr^{-1}).

from horizontal displacements (Models C1 and D1) are 7.8–18.0 ($\times 10^{20}$ Pa s), which are about two to five times of the values ($\sim$3.7 $\times 10^{20}$ Pa s) of upper mantle viscosity.

(5) Although the viscosity estimates of the transition zone from four-layer models verify the trend of depth-dependent viscosity in general, the STDs of the inversion computation are not significantly reduced from those of three-layer models. This suggests that the four-layer models do not provide a better fit to the GPS data than the three-layer models.

5.3 Results for earth models with more layers

Inversion computation has been carried out for earth models of more than four layers (up to 11 layers; not shown here). The results indicate that uncertainties in the estimated lower mantle viscosity increase dramatically when more layers are introduced. There is trade-off among the viscosity layers in the lower mantle: different combinations of layers with low and high values give an equivalent fit to the data, but the residuals are not significantly reduced

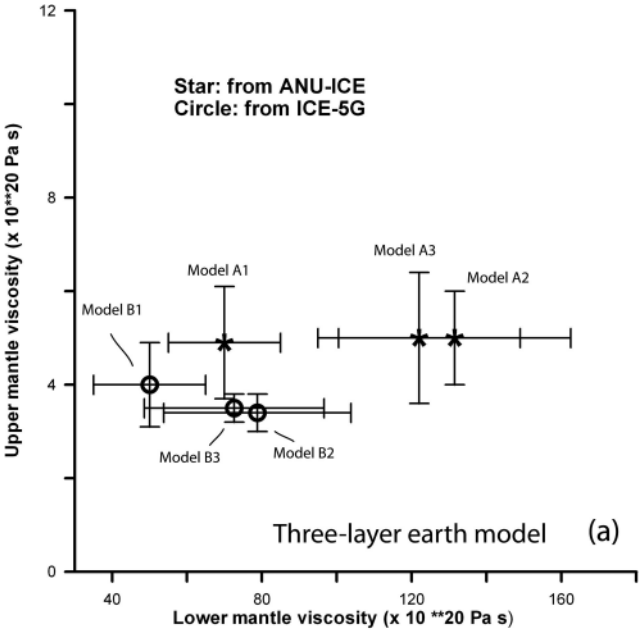

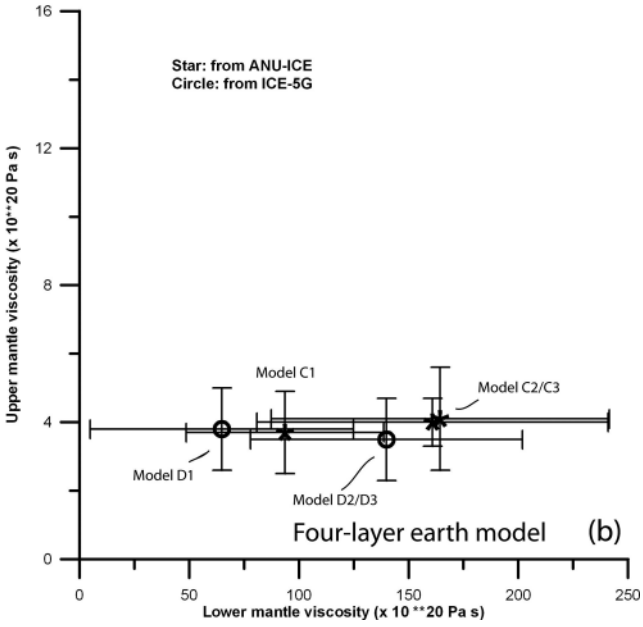

Figure 12. Uncertainties of mantle viscosity estimates from three- and four-layer earth models, respectively. Stars denote estimates from ANU-ICE, and circles are from ICE-5G (Ref. Tables 2 and 3).

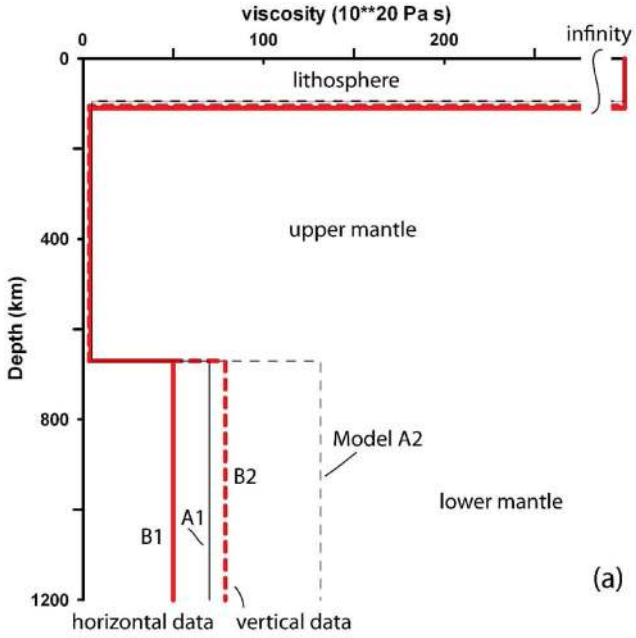

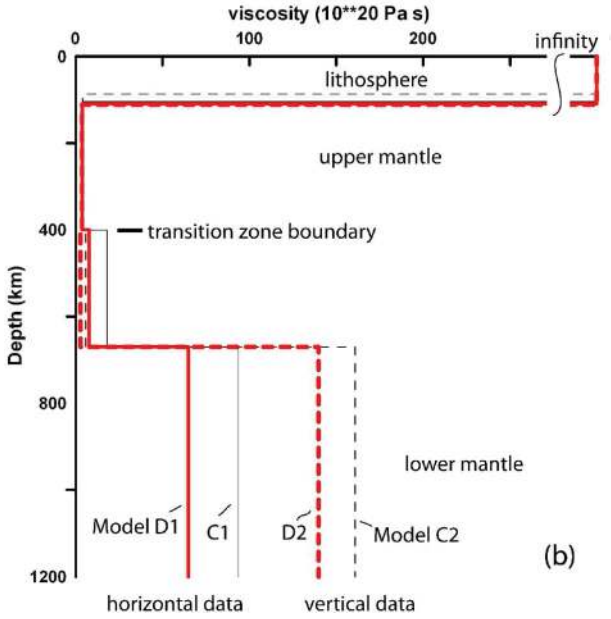

Figure 13. Earth models estimated from inversion analysis of GPS data with ANU-ICE and ICE-5G, respectively. (a) Three-layer earth model and (b) four-layer earth model (with a transition zone).

comparing with the three-layer model. Fig. 12 shows the uncertainties of mantle viscosity estimates from the inversion computation with three- and four-layer models. The uncertainties increased significantly in the lower mantle viscosity estimates after introducing the transition zone (see error bars in Fig. 12b). Therefore, the GPS data used in this study have no resolving power for more detailed layering structures in the mantle. A similar conclusion has been reported by Paulson *et al.* (2007), where it is shown that inversion computation with a Monte Carlo method cannot resolve more than two layers in the mantle from the gravity changes and relative sea-level data near Hudson Bay.

6 DISCUSSION

There are significant differences in the crustal deformation derived from the GPS solutions of 2007 and 2010 (Lidberg *et al.* 2007, 2010; see Fig. 1). The differences reflect errors in GPS solutions, which are associated with observational noise, systematic errors (of different reference systems), and errors in data processing procedures. The STDs estimated from the differences of the GPS solutions reveal that the nominal STDs have underestimated real errors by a factor of about 3 (Table 1). On the basis of the updated GPS solution (Lidberg *et al.* 2010), the earth model parameters are estimated from

Table 4. Observed and predicted deformation at two GPS sites in Tromsø, Norway.

Site	Longitude	Latitude	Time span	Observed (mm yr^{-1})			Predicted (Model A1) (mm yr^{-1})		
				u_e	u_n	u_z	U_e	U_n	U_z
TRO1	18.94	69.66	7.7	1.31	1.23	4.61	−0.278	0.593	4.15
TROM	18.938	69.663	7.9	0.17	0.58	4.15	−0.278	0.593	4.15

Note: U_e, U_n and U_z are predicted with Model A1 (Table 2)

Table 5. Parameters of the three-layer earth model in Fennoscandia from different studies.

Parameter	Lithosphere thickness (km)	Upper mantle viscosity (10^{20})	Transition zone viscosity	Lower mantle viscosity (10^{21})	Data used
Milne *et al.* 2004	∼100	5–10	NA	5–50	GPS (1993–2000)
Lambeck *et al.* (2010)	65–100	3–4	NA	5–20	Relative sea-level indicators
This study	93–110	3.4–5.0	Not resolved	7–13	GPS (1993–2006)

inversion of horizontal and vertical displacements separately and jointly with two different ice models (ANU-ICE and ICE-5G), respectively (Tables 2 and 3). Fig. 13 shows the earth model parameters estimated from horizontal and vertical deformation, respectively (the estimates from joint inversion are not shown here). The results demonstrate that estimated earth model parameters are affected by different data sets and ice models used. Uncertainties in ice sheet models are directly transferred into the inversion analysis because the ice configurations are fixed.

The differences in ice sheet models are mostly reflected in the estimates of lithosphere thickness and lower mantle viscosity. ICE-5G gave a lithosphere which is ∼10 km thicker (105–110 km) and a low value for the lower mantle viscosity (50.0×10^{20}–78.87×10^{20} Pa s), comparing with those from ANU-ICE (93–97 km; 70×10^{20}–120×10^{20} Pa s). The effects of observational errors in the inversion analysis could have been dwarfed by the effects of different ice sheet models. For example, the difference in the lower mantle viscosity estimated from vertical deformation between ICE-5G and ANU-ICE (Models B2 versus A2) is comparable to those due to different data sets with the same ice sheet (Models A1 versus A2 and Models B1 versus B2 in Fig. 13a).

There is a tendency that the lower mantle viscosity estimate from inversion of horizontal deformation is generally smaller than that from vertical deformation (solid versus dashed lines in Fig. 13). It is not clear whether this difference reflects that the horizontal and vertical displacements provide different constraints to the GIA models or is due to different noise levels in the data sets.

Comparing with the three-layer earth model, the four-layer earth model fit the GPS data equally well, and there is no significant reduction in residual STDs. This suggests that the earth model with a transition zone is not resolved by the GPS data. Adding more layers in the mantle increases non-uniqueness of the inversion computation to some extent, which results in large uncertainties in lower mantle viscosity estimates (Fig. 12b). The results partially verify the finding by Paulson *et al.* (2007) that current observations cannot resolve earth models with more than two layers in the mantle.

Inspecting the observed and predicted horizontal vectors (e.g. Figs 6a and 8a), the horizontal displacements in the south-eastern part of the region (South Finland) are underestimated: the predicted horizontal displacements are much smaller than those observed. It is not clear whether the relatively large horizontal deformation in the area is a genuine feature, because this feature was not present in previous GPS solutions (Johansson *et al.* 2002; Lidberg *et al.* 2007; see Fig. 1a). The magnitude of horizontal deformation in South Finland from the 2007 solution is about half of that from the 2010 solution (Fig. 1a). Future GPS observations may help to clarify this discrepancy. In addition, there are some horizontal displacements, which cannot be explained by the GIA models, especially for those sites along the west–southwest coast of the region. For example, there are significant differences in the horizontal deformation at two sites (TRO1 and TROM) about 350 m apart in the north-western corner of the region (Tromsø, Norway; see Fig. 1a). The observed and predicted displacements at the two sites are listed in Table 4. The magnitude of predicted horizontal displacements is in agreement with that observed at site TROM, while the large magnitude of horizontal displacements observed at site TRO1 is not consistent with the predictions. These anomalies might represent local deformation associated with coastal instability.

The effect of the North American ice sheets on the horizontal deformation in Fennoscandia has been ignored in this study. Modelling results show that the North American ice sheets produce an averaged shift of about 0.3 mm yr^{-1} on the GPS sites (Ref. Lambeck & Purcell 2003). However, such evaluation with the GIA process alone is subject to uncertainties due to the possible effects of plate boundaries and lateral heterogeneity in lithosphere/mantle (e.g. Klemann *et al.* 2008). In view of current accuracy of the horizontal deformation used in this study (Table 1), the effects of North American ice sheets and earth rotation (Argus & Peltier 2010) might have been masked by noise in GPS observations.

Finally, we take the results from the three-layer earth model as the representative estimates constrained by current GPS data. The estimates from ANU-ICE and ICE-5G define a narrow range of estimates (Table 2 and Fig. 13a): the effective lithosphere thickness of 93–110 km, upper mantle viscosity of 3.4×10^{20}–5.0×10^{20} Pa s, and lower mantle viscosity of 7×10^{21}–13×10^{21} Pa s. Although the upper mantle viscosity estimated from this study is smaller than that from Milne *et al.* (2004) (Table 5), these estimates are consistent with those inverted from relative sea-level indicators in Fennoscandia (Lambeck *et al.* 2010).

ACKNOWLEDGMENTS

We thank the Editor, John Dawson and an anonymous reviewer for their comments that improved the manuscript. S. Zhao publishes with the permission of the CEO, Geoscience Australia.

REFERENCES

Altamimi, Z., Sillard, P. & Boucher, C., 2002. ITRF2000: a newrelease of the International Terrestrial Reference Frame for earth science applications, *J. geophys. Res.,* **107**(B10), 2214, doi:10.1029/2001JB000561.

Altamimi, Z., Sillard, P. & Boucher, C., 2003. The impact of a No-Net-Rotation Condition on ITRF2000, *Geophys. Res. Lett.,* **30**(2), 1064, doi:10.1029/2002GL016279.

Altamimi, Z., Collilieux, X., Legrand, J., Garayt, B. & Boucher, C., 2007. ITRF2005: a new release of the International Terrestrial Reference Frame based on time series of station positions and earth orientation parameters, *J. geophys. Res.,* **112,** B09401, doi:10.1029/2007JB004949.

Altamimi, Z., Collilieux, X. & Metivier, L., 2011. ITRF2008: an improved solution of the International Terrestrial Reference Frame, *J. Geodyn.,* **85,** 457–473.

Argus, D.F., 2007. Defining the translational velocity of the reference frame of Earth, *Geophys. J. Int.,* **169,** 830–838, doi:10.1111/j.1365-246X.2007.03344.x.

Argus, D.F. & Peltier, W.R., 2010. Constraining models of postglacial rebound using space geodesy: a detailed assessment of model ICE-5G (VM2) and its relatives, *Geophys. J. Int.,* **181,** 697–723.

Braun, A., Kuo, C.Y., Shum, C.K., Wu, P., van der Wal, W. & Fotopoulos, G., 2008. Glacial isostatic adjustment at the Laurentide ice sheet margin: models and observations in the Great Lakes region, *J. Geodyn.,* **46,** 165–173.

Dziewonski, A.M. & Anderson, D.L., 1981. Preliminary reference earth model (PREM), *Phys. Earth Planet. Inter.,* **25,** 297–356.

Fleming, K. & Lambeck, K., 2004. Constraints on the Greenland ice-sheet since the last glacial maximum from observations of sea-level change and glacial rebound modeling, *Quat. Sci. Rev.,* **23,** 1053–1077.

Gabasov, R.F. & Kirillova, F.M., 1988. *Methods of Optimization,* Optimization Software Inc., New York, NY, 364pp.

Johansson, J.M. *et al*., 2002. Continuous GPS measurements of post-glacial adjustment in Fennoscandia 1. Geodetic results, *J. geophys. Res.,* **1079**(B8), doi:10.1029/2001B000400.

Johnston, P. & Lambeck, K., 1999. Postglacial rebound and sea level contributions to changes in the geoid and the Earth's rotation axis, *Geophys. J. Int.,* **136,** 537–588.

Klemann, V., Martinec, Z. & Ivins, E.R., 2008. Glacial isostasy and plate motions, *J. Geodyn.,* **46,** 95–103.

Lambeck, K. & Johnston, P., 1998. The viscosity of the mantle: evidence from analyses of glacial rebound phenomena, in *The Earth's Mantle,* pp. 461–502, ed. Jackson, I., Cambridge University Press, Cambridge.

Lambeck, K. & Purcell, A., 2003. *Glacial Rebound and Crustal Stress in Finland, POSIVA 2003–10,* Olkiluoto, Finland, 84pp.

Lambeck, K., Purcell, A., Johnston, P., Nakada, M. & Yokoyama, Y., 2003. Water-load definition in the glacio-hydro-isostatic sea-level equation, *Quat. Sci. Rev.,* **22,** 309–318.

Lambeck, K., Purcell, A., Zhao, J. & Svensson, N.-O., 2010. The Scandinavian ice sheet: from MIS 4 to the end of the last glacial maximum, *Boreas,* **39,** 410–435.

Lambeck, K., Smither, C. & Johnston, P., 1998. Sea-level change, glacial rebound and mantle viscosity for northern Europe, *Geophys. J. Int.,* **134,** 102–144.

Lidberg, M., Johansson, J.M., Scherneck, H.G. & Davis, J.L., 2007. An improved and extended GPS-derived 3D velocity field of the glacial isostatic adjustment (GIA) in Fennoscandia, *J. Geodesy.,* **81,** 213–230, doi:10.1007/s0019000601024.

Lidberg, M., Johansson, J.M., Scherneck, H.G. & Milne, G., 2010. Recent results based on continuous GPS observations of the GIA process in Fennoscandia from BIFROST, *J. Geodyn.,* **50,** 8–18.

Milne, G.A., Davis, J.L., Mitrovica J.X., Scherneck, H.-G., Johansson, J.M., Vermeer, M. & Koivula, H., 2001. Space-geodetic constraints on glacial isostatic adjustments in Fennoscandia, *Science,* **291,** 2381–2385.

Milne, G.A., Mitrovica, J.X., Scherneck, H.-G., Davis, J.L., Johansson, J.M., Koivula, H. & Vermeer, M., 2004. Continuous GPS measurements of postglacial adjustment in Fennoscandia: 2. Modeling results, *J. geophys. Res.,* **109,** B02412, doi:10.1029/2003JB002619.

Mitrovica, J.X. & Milne, G.A., 1998. Glaciation-induced perturbations in the Earth's rotation: a new appraisal, *J. geophys. Res.,* **103,** 985–1005.

Nakada, M. & Lambeck, K., 1987. Glacial rebound and relative sea-level variations: a new appraisal, *Geophys. J. R. Astron. Soc.,* **90,** 171–224.

Paulson, A., Zhong, S. & Wahr, J., 2007. Inference of mantle viscosity from GRACE and relative sea level data, *Geophys. J. Int.,* **171,** 497–508.

Peltier, W.R., 1974. The impulse response of a Maxwell Earth, *Rev. Geophys.,* **12,** 649–669.

Peltier, W.R., 1985. The LAGEOS constraint on deep mantle viscosity: results from a new normal mode method for the inversion of viscoelastic relaxation spectra, *J. geophys. Res.,* **90,** 9411–9421.

Peltier, W.R., 2002. Global glacial isostatic adjustment: paleogeodetic and space- geodetic tests of the ICE-4G (VM2) model, *J. Quat. Sci.,* **17**(5–6), 491–510.

Peltier, W.R., 2004. Global glacial isostasy and the surface of the ice-age earth: the ICE-5G (VM2) model and GRACE, *Ann. Rev. Earth Planet. Sci.,* **32,** 111–149.

Peltier, W.R. & Andrews, J.T., 1976. Glacial isostatic adjustment-I. The forward problem, *Geophys. J. R. Astron. Soc.,* **46,** 605–646.

Sabadini, R. & Vermeersen, B., 1997. Ice-age cycles: earth's rotation instabilities and sea-level changes, *Geophys. Res. Lett.,* **24,** 3041–3044.

Steffen, H. & Wu, P., 2011. Glacial isostatic adjustment in Fennoscandia: a review of data and modelling, *J. Geodyn.,* **52,** 169–204.

Tushingham, A.M. & Peltier, W.R., 1991. ICE-3G: a new global model of late Pleistocene deglaciation based upon geophysical predictions of post-glacial relative sea level change, *J. geophys. Res.,* **96,** 4497–4523.

Vink, A., Steffen, H., Reinhardt, L. & Kauffmann, G., 2007. Holocene relative sea-level change, isostatic subsidence and the radial viscosity structure of the mantle of northwest Europe (Belgium, the Netherlands, Germany, southern North Sea), *Quat. Sci. Rev.,* **26,** 3249–3275.

Wu, P. & Peltier, W.R., 1982. Viscous gravitational relaxation, *Geophys J. R. Astron. Soc.,* **70,** 435–85.

Wu, X.P. *et al*., 2010. Simultaneous estimation of global present-day water transport and glacial isostatic adjustment, *Nat. Geosci.,* **3**(9), 642–646, doi:10.1038/ngeo938.